A Six-Port Automatic Network Analyzer

HARRY M. CRONSON, SENIOR MEMBER, IEEE, AND LEON SUSMAN, SENIOR MEMBER, IEEE

Abstract—**This paper describes the analysis, design, and testing of a six-port automatic network analyzer. A new calibration procedure is derived from a matrix description of the six-port network. The calibration constants appear as the solution of an eigenvalue problem resulting in new insights and faster numerical computation. A programmable calculator-controlled six-port system was designed to measure S_{11} and S_{21} over the frequency range 2–18 GHz without perturbing the device under test. Measurements on the completed system taken from 7–12 GHz show that results within 1 percent can be obtained.**

I. Introduction

THE NEED FOR wide band, accurate, fast, and inexpensive microwave measurement of S-parameters has been growing at a rapid rate. Although the computer-controlled automatic network analyzer satisfies the first three characteristics, it carries a high price tag. Recent work at the National Bureau of Standards (NBS) [1], [2] on programmable calculator-controlled six-port measurement systems has shown promise in reducing the cost of automated measurements without sacrificing accuracy. Expanding on the NBS work, we have critically examined the analytical basis for the calibration and measurement procedures and built a prototype six-port automated network analyzer (SPANA) designed to demonstrate the feasibility of measuring both S_{21} and S_{11} from 2–18 GHz.

The main feature of the technique is that a six-port network, with square-law detectors on the four output ports, can be calibrated to determine the amplitude and phase of the ratio of signals at the two input ports. This complex ratio of input signals is calculated from the six-port network constants and the output detector voltages. The simplicity of the microwave detection process reduces the cost of components needed for the usual frequency conversion methods, and permits automation via a programmable calculator-based system.

The work described in this paper has contributed to the six-port state-of-the-art in both analysis and hardware realizations. On a conceptual level the matrix description has led logically to a new calibration approach. From our analysis we formulate the calibration equations as an eigenvalue problem; this results in a simpler and faster computer program. The prototype analyzer has several important advantages over previous NBS systems. The SPANA combines reflection and insertion loss measurements in one unit without disturbing the device under test (DUT). The amount of hardware has been substantially reduced with the elimination of banks of isolators. A more detailed description of this investigation is contained in a recently issued report [3].

Manuscript received May 16, 1977; revised July 17, 1977. This work supported by the U.S. Army Metrology and Calibration Center, US Army Missile Command, Redstone Arsenal, AL, under Contract DAAH01-75-C-1112.

The authors are with Sperry Research Center, Sudbury, MA 01776.

II. Matrix Description of the Six-Port Network

The measurement potential of a six-port network can best be appreciated by adopting a scattering matrix description. Consider the arbitrary six-port network shown in Fig. 1 with incident scattering variables a_i and reflected scattering variables b_i at the two input ports 1 and 2, and output ports 3–6. If each output port β is terminated in a power detector with reflection coefficient Γ_β, so that $a_\beta = \Gamma_\beta b_\beta$, the output variables b_β can be written as a linear combination of two remaining input variables such as a_1 and a_2 or a_2 and b_2. These four equations can then be written as

$$\vec{b}_\beta = A_\beta a_1 + B_\beta a_2 = C_\beta a_2 + D_\beta b_2 \tag{1}$$

where $\vec{b}_\beta$ denotes a column vector with entries b_β. The scalars $A_\beta, \cdots, D_\beta$ depend on the actual topology of the six port, that is the scattering matrix $\tilde{S}$. Since the net output power P_β at each output port is proportional to $|b_\beta|^2$, these four powers can be written in two alternate matrix forms

$$\vec{P} = \tilde{C}_I^{-1}\vec{a}_q \qquad \vec{P} = \tilde{C}_R^{-1}\vec{b}_q \tag{2}$$

where $\vec{P}$ is a column matrix of power readings and $\vec{a}_q$, $\vec{b}_q$ are column matrices containing certain quadratic functions of the input variables. Our notation requires some additional comment. The subscripts I and R are used for insertion loss and reflection coefficient, respectively. The entries of $\tilde{C}_I$ and $\tilde{C}_R$ are different as is the topology of the networks used in the two applications. In addition the tilde denotes a square matrix; A^T, $\tilde{A}^{-1}$ denote the transpose and inverse of matrix A, respectively. Specifically the entries of $\vec{a}_q$ and $\vec{b}_q$ can be taken as $|a_1|^2, a_1a_2^*, a_1^*a_2, |a_2|^2$. This formulation (which is used for convenience in the Appendix) requires that the entries of $\tilde{C}$ be complex. Alternately we may define $\vec{a}_q$, $\vec{b}_q$ as

$$\vec{a}_q = \begin{bmatrix} |a_1|^2 \\ \text{Re}\,(a_1a_2^*) \\ \text{Im}\,(a_1a_2^*) \\ |a_2|^2 \end{bmatrix}; \qquad \vec{b}_q = \begin{bmatrix} |b_2|^2 \\ \text{Re}\,(b_2a_2^*) \\ \text{Im}\,(b_2a_2^*) \\ |a_2|^2 \end{bmatrix} \tag{3}$$

where $\tilde{C}_I^{-1}$ and $\tilde{C}_R^{-1}$ are 4×4 real matrices of unknown proportionality constants. Equation (2) is a function rule relating certain input quadratics to the power readings. These equations completely describe the network properties we can observe with power meters at the four output ports.

If the matrix C^{-1} can be inverted, the input quadratics can be related directly to the power readings yielding

$$\vec{a}_q = \tilde{C}_I\vec{P} \qquad \vec{b}_q = \tilde{C}_R\vec{P}. \tag{4}$$

The entries of $\tilde{C}_R$ and $\tilde{C}_I$ are the calibration constants of the two network configurations whose values are deduced during the calibration procedure. Once the entries C_{ij} of

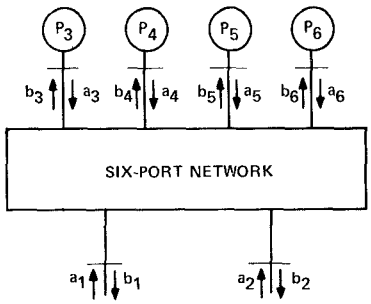

Fig 1. An arbitrary network with power meters on four of the six ports.

matrix $\underset{\sim}{C}$ are known to within a constant multiplier, a ratio of the input quadratics can be computed from (4) by simply measuring the output powers. For example, from (3), we obtain

$$\frac{a_2}{a_1} = \frac{a_2 a_1^*}{|a_1|^2} = \frac{\sum_{i=1}^{4} (C_{2i} - jC_{3i})P_i}{\sum_{i=1}^{4} C_{1i}P_i} \tag{5}$$

with a similar equation for a_2/b_2.

III. Calibration Procedure

There are two types of calibration procedures for determining the entries C_{ij}. For example, standards can be used to introduce known terminal conditions from which the calibration constants can be deduced. We have used this procedure in S_{11} measurements. An exposition of this method using a matrix description has appeared elsewhere [4].

Alternatively, there are self-calibration methods where no standards are necessary with the obvious advantage that no recalibration of the standard is required. The self-calibration technique reported by Hoer [1] for a six-port ratio meter is directly applicable to the measurement of S_{21}. Although no standards are required, use is made of a repeatable, but otherwise unknown, two position insertion device which inserts a complex attenuation L into one of the input channels. The calibration procedure consists of the following steps. With the two position insertion device in its "out" position, the four output powers are measured. We denote the column vector of such power readings as $\vec{P}$. This measurement is repeated for at least $m \geq 4$ different ratios of input excitations a_2/a_1. The resulting power readings are stored, by columns, in a matrix P. The measurements are repeated with the insertion device in the "in" position and the power readings are stored in matrix P'. It is assumed that the sole influence of the two states of the insertion device is to change one input channel from, say, a_2 to La_2 while a_1 remains constant. This procedure yields m equations of the form

$$L = \frac{a_2'}{a_2} = \frac{a_2' a_1'^*/|a_1'|^2}{a_2 a_1^*/|a_1|^2} = \frac{\sum_{i=1}^{4} [C_{2i} - jC_{3i}]P_i'}{\sum_{i=1}^{4} [C_{2i} - jC_{3i}]P_i} \tag{6}$$

where we have used (5) and the restriction $a_1 = a_1'$. These m nonlinear simultaneous equations can be solved in any number of ways. NBS has approached this problem by using an iterative technique based on a Taylor expansion of (6) about the correct values for the unknowns C_{2i}, C_{3i}, and L. When we examined this algorithm certain mathematical and conceptual difficulties were found which are clarified when the eigenvalue nature of the equation is recognized.

It is shown in Appendix A (equation (A-7)) that the set of m equations given in (6) can be embedded in an eigenvalue problem. Specifically we show that

$$\underset{\sim}{C}^{T-1} \underset{\sim}{W}^T \underset{\sim}{C}^T = \underset{\sim}{C}^{T-1}[(PP^T)^{-1}PP'^T]\underset{\sim}{C}^T = \underset{\sim}{\Lambda} \tag{7}$$

where $\underset{\sim}{\Lambda}$ is a diagonal matrix and $\underset{\sim}{W}$ is defined by (7). In addition we are able to exhibit these eigenvalues explicitly, that is λ_i, the diagonal elements of $\underset{\sim}{\Lambda}$, under ideal terminal conditions, are 1, L, L^*, and $|L|^2$. Corresponding to each eigenvalue there is an associated eigenvector. The components of the eigenvector associated with $\lambda = L$ contain the calibration constants used in (5). Herein lies an explanation of the occasional failure of the NBS technique. If the initial guess at the calibration constant is poorly chosen, the NBS technique can converge to either $\lambda = 1, L^*$, or $|L|^2$, and their associated eigenvector rather than the eigenvalue of interest $\lambda = L$. In addition, since L and L^* are complex conjugates, we must have some means of deciding which eigenvalue and eigenvector has actually been computed. To put it another way we must know the sign of L *a priori*.

The recognition of (7) as an eigenvalue problem has lead to an entirely different numerical algorithm which requires far fewer mathematical operations. The execution time is much faster and the computer storage involved is greatly reduced. A program using this eigenvalue approach has been developed and was used with the SPANA for measurements of S_{21}.

The new technique is based on the observation that since L represents the value of an attenuator we can identify 1 and $|L|^2$ as the maximum and minimum eigenvalues. These can be found directly from the matrix $\underset{\sim}{W}^T$; that is from the power measurements, by a simple iterative technique [5]. From the additional fact that the trace of $\underset{\sim}{W}^T$ must be equal to the sum of the eigenvalues, and the determinant of $\underset{\sim}{W}^T$ must be equal to the product of the eigenvalues, we can find all the eigenvalues to within a sign ambiguity for L and L^*. Once the complete eigenvalue set has been found, the eigenvectors associated with any of the eigenvalues, say λ_4 for example, can be found by forming the adjoint of $(\underset{\sim}{W}^T - \lambda_4 I)$. It can be shown that the eigenvectors associated with λ_4 can be taken to be proportional to the nonzero columns of Adj $(\underset{\sim}{W}^T - \lambda_4 I)$. A simple expression for this matrix function makes this calculation straightforward [6]

$$\text{Adj}\,(\underset{\sim}{W}^T - \lambda_k I) = \prod_{\substack{i=1 \\ i \neq k}}^{4} (\underset{\sim}{W}^T - \lambda_i I). \tag{8}$$

Finally we note that the actual calculation uses the measured data, the entries of $\underset{\sim}{W}$. We thus expect that the calculated maximum eigenvalue will be only approximately 1. In fact the departure of λ_1 from its ideal value is a measure of our ability to keep $|a_1|^2 = |a_1'|^2$.

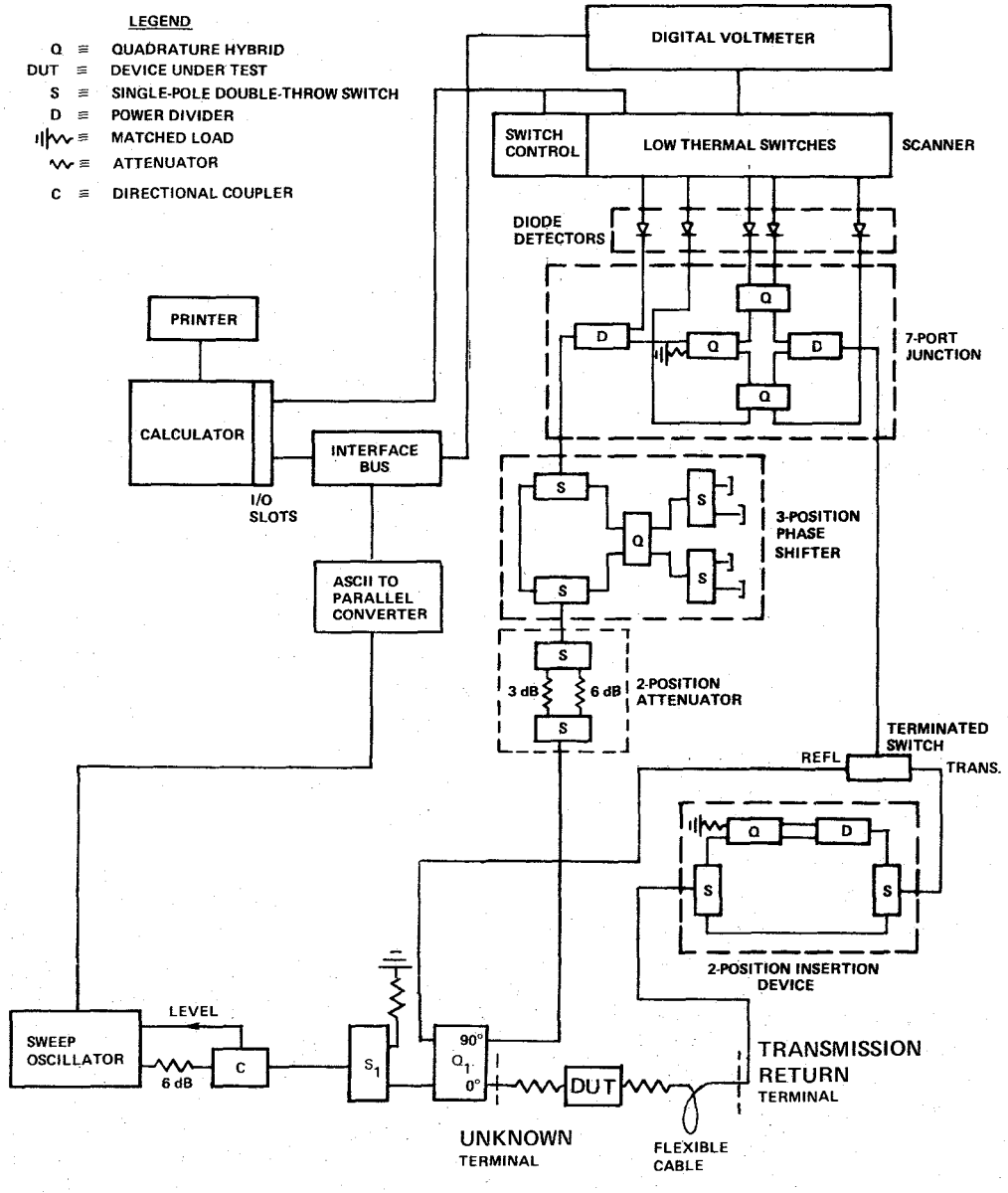

Fig. 2. Schematic diagram of SPANA.

IV. System Description

A block diagram of the SPANA is shown in Fig. 2. The entire system is under control of a programmable calculator which performs all the required computations, and through its interface bus controls all of the RF switching. The RF components are designed to operate over the entire 2–18 GHz frequency range. Special components included for self-calibration in the S_{21} mode are the two-position insertion device and the three-position phase shifter/two-position attenuator combination, used to vary the input excitation ratio to the seven-port network.

The sweep oscillator, under calculator control, supplies CW signals at selected frequencies to the microwave network. An external leveling loop is added to increase stability. Since it is desired to obtain background voltage levels during the measurement and calibration procedure,

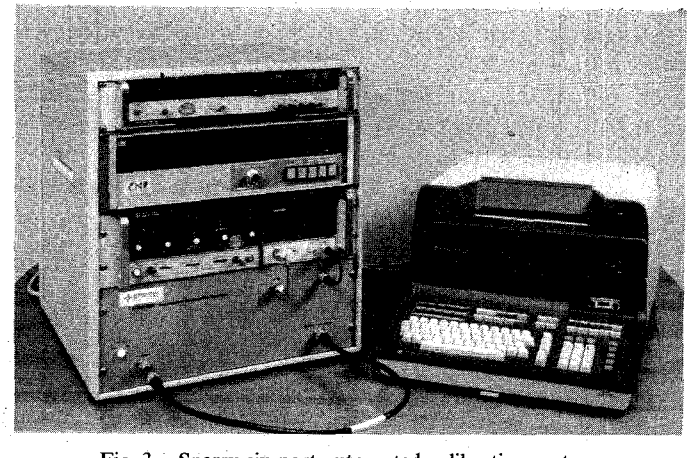

Fig. 3. Sperry six-port automated calibration system.

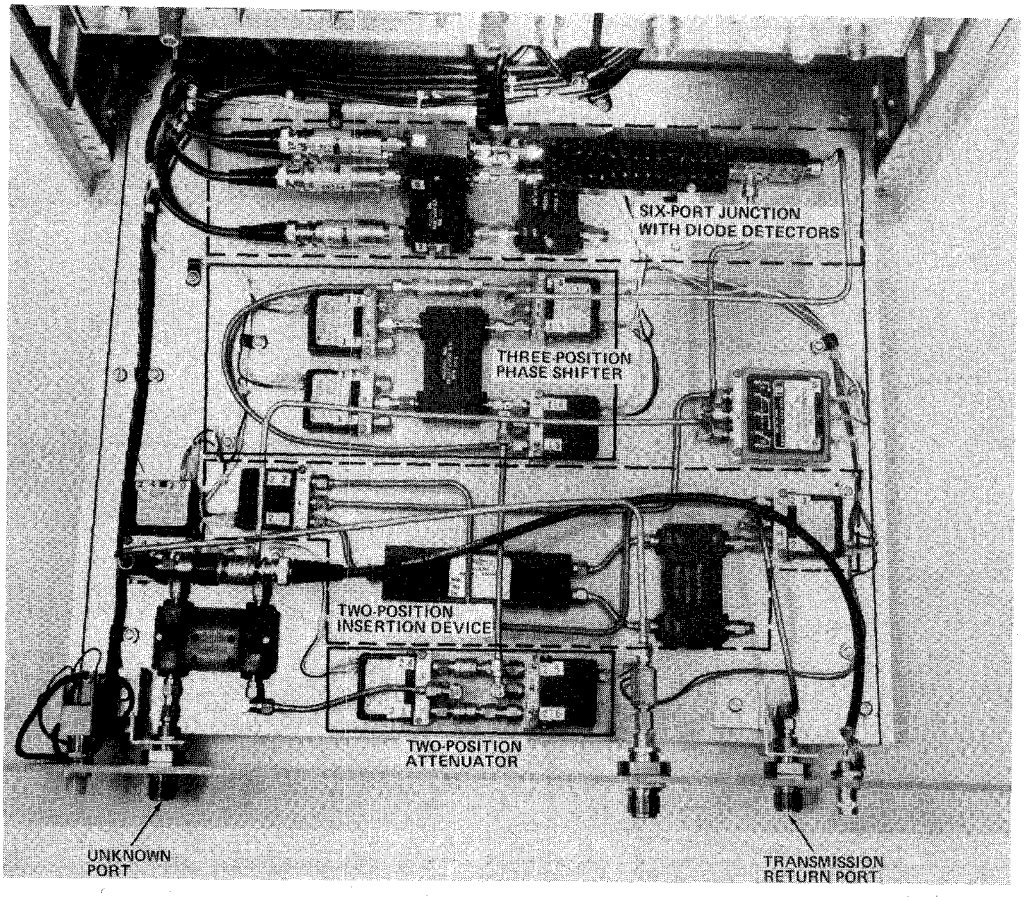

Fig. 4. Sperry six-port microwave network.

an RF single-pole double-throw switch S_1 is used to direct power away from the network and into a matched load.

The Q hybrid Q_1 following the switch S_1 is used as a 3-dB dual-directional coupler. The signal from the $-90°$ port is connected to the seven-port network as a reference waveform. The isolated port wave is an essential part of the reflectometer network. An insertion point for the DUT is connected to the 0° port. For S_{21} measurements, attenuators are placed on both sides of the DUT to improve the match. Various standards for calibrating the reflectometer are also inserted at this position. A precision flexible cable is included for allowing a variety of devices to be connected between the test ports. The two-position insertion device used in the self-calibration procedure follows the NBS design for a component with 3-dB insertion loss and 45° phase shift. The signal from this device is connected to one input of a terminated switch. The isolated port wave from Q_1 serves as the other input. Either the reflected or transmitted signal can then be selected as one input to the seven-port junction.

Redirecting attention to Q_1, the 90° output signal passes through the components used in the self-calibration procedure before it enters into the other input port of the seven-port junction. The first is a two-position step attenuator, and the other is a three-position phase shifter of NBS design.

In the seven-port junction only four output ports are used at any time. The additional port is available so that different port combinations may be evaluated for different conditions. The five outputs from the seven-port junction are terminated in diode detectors with load resistors chosen for optimum square-law response up to as large an input power as possible. The five output voltages from the diodes are fed into a scanner which selects individual voltages for the digital voltmeter. Other relays in the scanner are used to open and close the RF switches. For simplicity, the control lines from the scanner to the switches are not shown. To allow the calculator to communicate with the instruments an interface bus system is used. The bus is directly interfaced to the digital voltmeter and indirectly to the sweeper through a converter. The scanner is connected directly to the calculator through an input–output interface.

An overall photograph with the instrument cabinet and calculator is shown in Fig. 3. In the cabinet from top to bottom are the DVM, scanner, sweeper, and microwave rack. Fig. 4 is a close-up view of the microwave networks with the pertinent subassemblies called out.

V. Measurement Procedure and Results

A self-calibration procedure is employed for S_{21} measurements. Under calculator control, sets of diode output voltages are acquired and stored with the two-position insertion device in each state for each of six possible combinations of the two-position attenuator and three-position phase shifter. From these readings, the six-port

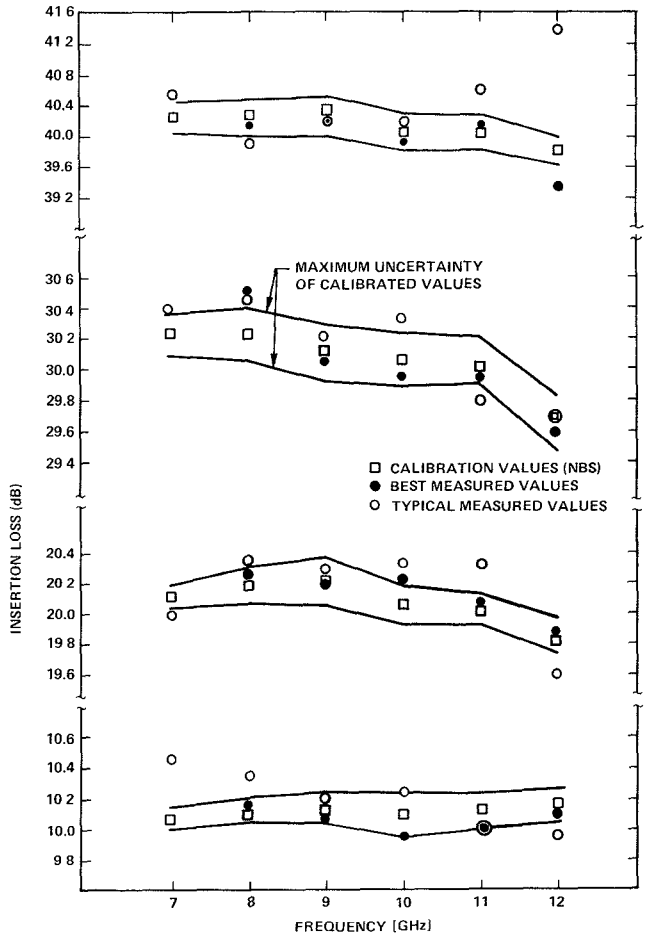

Fig. 5. Six-port insertion loss measurement at 10, 20, 30, and 40 dB.

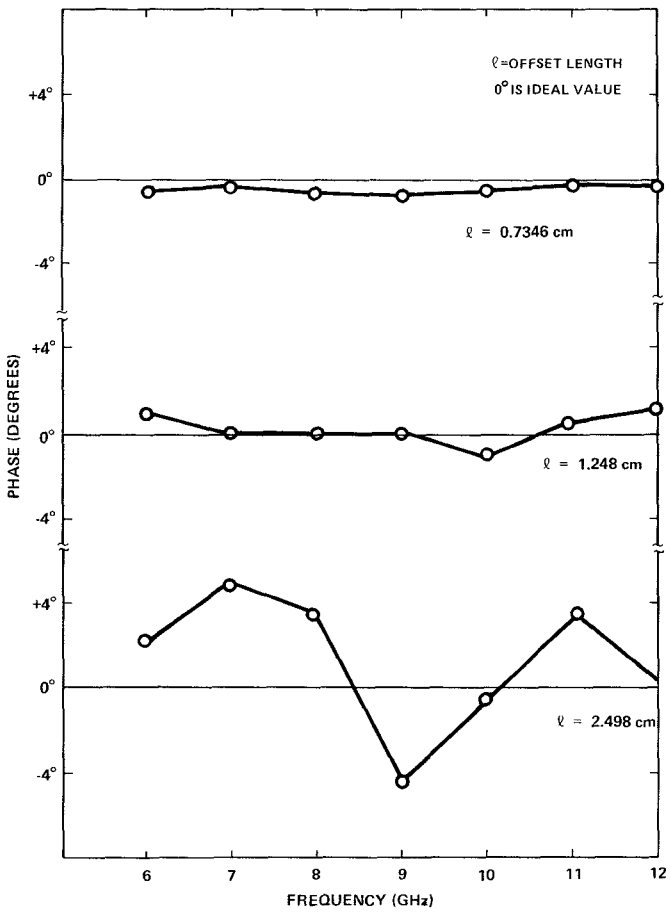

Fig. 6. Deviation from ideal phase values for offset shorts.

calibration constants for the S_{21} mode are determined using an eigenvalue approach. The six-port reflectometer constants are found using four standards at the unknown terminal: a matched load, a short, and two offset shorts. Once calibration is complete, the S_{21} of a DUT is determined in three steps. First a through measurement without the DUT is performed. Next, the two output terminals are connected to matched loads in order to obtain a correction term for the effect of leakage through the six-port junction. Then the DUT is connected and measurements taken. The three sets of four diode voltage measurements are then used with the calibration constants to compute the unknown S_{21}. The S_{11} of the DUT is found by switching internally to the reflectometer mode and acquiring the four diode voltages. After all voltages are acquired the calculator computes and prints S_{21} and S_{11} for each test frequency.

Although the six-port system was designed to cover the 2–18 GHz range, measurements were made only from 6–12 GHz because we did not have access to sweepers outside this range during the test period. The results of two of the measurement runs on coaxial attenuators are illustrated in Fig. 5 with three different sets of data points. One set is the insertion loss values along with bounds for the maximum uncertainty as calibrated by NBS. A second set shows the best six-port data selected from about five runs taken on different days. Here the criterion for best was the data closest to the calibration values. A third set illustrates the scatter for a more typical run. This data demonstrates the good agreement between the best run and the calibrated values. The scatter increased somewhat for 40 dB and was poor at 50 dB.

Fig. 6 shows the measured deviation from ideal phase for three offsets is within 1° and deteriorates to almost 5° for the longest one.

VI. Discussion

Measurements on the SPANA from 7–12 GHz have demonstrated that results within 1 percent can be achieved, although typical runs give somewhat lesser accuracies. Clearly, questions on system errors need to be resolved to explain these differences. A preliminary investigation indicated that mismatch uncertainty due to finite source and load reflection coefficients was the largest source of attenuation errors. This could be reduced by implementing a hardware change that would allow measurement of the reflection coefficients looking into the two ports of the analyzer. Subsequent software procedures could then be used to make the necessary corrections. We also later discovered that a connector on the flexible cable was faulty during the tests which could account for some of the erratic results.

An alternate approach, which obviates mismatch correc-

tions, by using two six-port junctions, one on each side of the DUT, has been recently proposed by Hoer [7]. Further progress in developing practical six-port analyzers will probably be based on multi-six-port systems and will depend on a greater understanding of their calibration procedures and error sources.

Appendix A
Self-Calibration Equations for the Six Port

In this Appendix we wish to review the mathematical basis for viewing the self-calibration procedure as an eigenvalue problem. We showed in (4) that the quadratics associated with the input excitations are related to the power meter readings by

$$\vec{a}_q = \underset{\sim}{C}\vec{P}. \tag{A-1}$$

It will simplify the subsequent analysis to use the complex formulation for the quadratic variables. Thus the entries of $\underset{\sim}{C}$ are in general complex numbers, and $\underset{\sim}{C}$ is assumed to be nonsingular. In the NBS self-calibration procedure an insertion device is placed in tandem with port 2. This produces new incident scattering variables a'_1 and a'_2 with corresponding output power vector $\vec{P}'$. Thus a new set of input–output equations, similar to (A-1), results

$$\vec{a}'_q = \underset{\sim}{C}\vec{P}'. \tag{A-2}$$

If we assume that the insertion device simply changes the input variable from a_2 to $a'_2 = La_2$, and that a_1 remains constant, $a'_1 = a_1$, then we can summarize these terminal requirements by

$$\vec{a}'_p = \underset{\sim}{\Lambda}\vec{a}_q$$

where

$$\underset{\sim}{\Lambda} = \begin{bmatrix} 1 & 0 & 0 & 0 \\ 0 & L^* & 0 & 0 \\ 0 & 0 & L & 0 \\ 0 & 0 & 0 & |L|^2 \end{bmatrix}. \tag{A-3}$$

Since (A-1) through (A-3) are valid for each of m measurements, we can write the three augmented matrix equations

$$\begin{aligned} A_q &= \underset{\sim}{C}P \\ A'_q &= \underset{\sim}{C}P' \\ A'_q &= \underset{\sim}{\Lambda}A_q \end{aligned} \tag{A-4}$$

where A_q, A'_q, P, P' are $4 \times m$ matrices whose columns are the quadratic expressions and corresponding power readings shown explicitly in (A-1) and (A-2). $\underset{\sim}{C}$ and $\underset{\sim}{\Lambda}$ are the 4×4 calibration matrix and a diagonal matrix. Equation (A-4) can be used to eliminate A_q and A'_q resulting in the following matrix relationship,

$$\underset{\sim}{C}P' = \underset{\sim}{\Lambda}\underset{\sim}{C}P. \tag{A-5}$$

It follows from (A-5) that Λ is similar to the matrix $\underset{\sim}{W}$ defined by

$$\underset{\sim}{C}\underset{\sim}{W}\underset{\sim}{C}^{-1} = \underset{\sim}{\Lambda} = \underset{\sim}{C}[P'P^T(PP^T)^{-1}]\underset{\sim}{C}^{-1}. \tag{A-6}$$

The eigenvalues of $\underset{\sim}{W}'$ are thus the diagonal entries of $\underset{\sim}{\Lambda}$. Finally since $\underset{\sim}{\Lambda}$ is a diagonal matrix, we find that the transpose of $\underset{\sim}{\Lambda}$ is

$$\underset{\sim}{\Lambda}^T = \underset{\sim}{\Lambda} = \underset{\sim}{C}^{T-1}\underset{\sim}{W}^T\underset{\sim}{C}^T = \underset{\sim}{C}^{T-1}[(PP^T)^{-1}PP'^T]\underset{\sim}{C}^T \tag{A-7}$$

which shows directly that the rows of $\underset{\sim}{C}$, that is, our desired calibration constants, are the eigenvectors of $\underset{\sim}{W}^T$.

To facilitate comparison with Hoer's notation [1], [2], we remark that the eigenvector associated with $\lambda = 1$ is simply the $\vec{w}$ vector, the eigenvector associated with $\lambda = L$ is simply the $\vec{z}$ vector, and finally the eigenvector associated with $\lambda = |L|^2$ is the $\vec{\sigma}$ vector.

Acknowledgment

The authors appreciate the support and encouragement of F. Seeley and M. Shelton of the Army Metrology and Calibration Center, Huntsville, AL, and the cooperation of C. Hoer and G. Engen of NBS, Boulder, CO.

References

[1] C. A. Hoer and K. C. Roe, "Using an arbitrary six-port junction to measure complex voltage ratios," *IEEE Trans. Microwave Theory Tech.*, vol. MTT-23, pp 978–984, Dec. 1975.
[2] C. A. Hoer, "Using six-port and eight-port junctions to measure active and passive circuit parameters," *NBS Tech. Note 673*, Sept. 1975.
[3] H. M. Cronson and L. Susman, "Automated six-port microwave calibration system," Final Tech. Rep., U.S. Army Missile Command, Redstone Arsenal, AL, SCRC-CR-77-32, Apr. 1977.
[4] ——, "A new calibration technique for automated broadband microwave measurements," in *Proc. 6th Annu. Eur. Microwave Conf.* (Rome, Italy), Sept. 1976.
[5] F H. Hildebrand, *Methods of Applied Mathematics*. Englewood Cliffs, NJ: Prentice-Hall, Inc., 1952, pp. 68–82.
[6] R. A. Frazer, W. J. Duncan, and A. R. Collar, *Elementary Matrices*. New York: Cambridge, 1960.
[7] C. A. Hoer, "A network analyzer using two six-port reflectometers," this issue, pp. 1070–1074.